

Optical Measurement of Photorecombination Time Delays

Chunmei Zhang*, Graham G. Brown*, Dong Hyuk Ko, Paul B. Corkum

Joint Attosecond Science Laboratory, University of Ottawa and National Research Council of Canada, 100 Sussex Dr, Ottawa, Canada, K1N 6N5

Corresponding Author Email: graham.brown@uottawa.ca

*These authors contributed equally to this work

July 27, 2021

Measuring the photoionization time delay between electrons from different orbitals is one of the most important accomplishments of attosecond science¹. These measurements are typically done using attosecond pulses to photoionize a target inside a photoelectron spectrometer². In such experiments, the measured delay corresponds to the superposition of all possible paths to ionization and can include multiple sources of delay³⁻⁸. These effects can be difficult to deconvolve⁹. Here, we exploit the collision physics nature of recollision and show that, by perturbing recollision dynamics¹⁰, photorecombination time delays due to electron dynamics and structure can be measured entirely optically and without obfuscation from molecular structure¹¹ and propagation effects. While we concentrate on photorecombination delays in argon around the Cooper minimum⁶ our approach is general. Therefore, our work holds the potential to fundamentally change how attosecond measurement¹² is performed and paves the way for the entirely optical measurement of ultrafast electron dynamics and photorecombination delays due to electronic structure, multielectron interaction, and strong-field driven dynamics in complex molecular systems and correlated solid-state systems.

Cooper minima are ubiquitous in photoionization spectra from atoms and molecules¹³. The dipole transition matrix element coupling continuum states to a ground state wavefunction exhibiting a radial node passes through zero, leading to a spectral minimum and corresponding phase jump in photoionization spectra. The rapid phase variation across a Cooper minimum gives rise to significant photoionization time delays which have been measured using attosecond techniques¹⁴. As the inverse process of photoionization, photorecombination also exhibits Cooper minima, most notably in high-harmonic generation (HHG)¹⁵⁻¹⁷. The spectral phase of attosecond pulses generated by recollision in such media is significantly shaped by photorecombination time delays around Cooper minima⁶.

Photoionization time delays are typically measured using attosecond pulses to photoionize a target within a photoelectron spectrometer. In addition to the equipment used for attosecond pulse generation, these measurements require a phase locked infrared probe pulse that is adjustable with attosecond precision with respect to the attosecond pulse, an XUV filter to separate the attosecond pulse from the driver beam which lowers the attosecond pulse intensity, and XUV optics for attosecond beam refocusing and attosecond-infrared beam recombination

that are applied in the electron spectrometer¹⁸. Further, there are several possible sources of delay which can include molecular or electronic structure, field-driven electron dynamics, and dispersive propagation effects³⁻⁸. Consequently, interpretation can be ambiguous.

Here, we report an approach to studying ultrafast electron dynamics and photorecombination time delays that melds the precision of optics with collision physics. That is, we manipulate the electron-ion collision with a perturbing field while observing the results optically. This approach, often called *in situ* measurement, permits us to measure photorecombination time delays that originate from many sources. It is commonly accepted, however, that *in situ* measurement is incapable of measuring photorecombination time delays¹¹. Here, we demonstrate the viability of *in situ* measurement by studying the recombination phase around the Cooper minimum in argon experimentally while also confirming our interpretation using time-dependent density functional theory¹⁹ (TD-DFT) simulations (please see supplementary information). We then use the semi-classical strong field approximation²⁰ (SFA) description of recollision (please see supplementary information) to show that *in situ* methods are insensitive to phase originating from the molecular structure.

The process of recollision leading to attosecond pulse emission consists of three steps²¹: (1) in the presence of a strong field, an electron tunnels into the continuum, (2) the electron is accelerated by the strong field, and (3) the electron recombines with its parent ion and emits an attosecond pulse. In sinusoidal fields, these three-steps repeat every half optical-cycle, resulting in an attosecond pulse train²⁰.

We generate an isolated attosecond pulse in argon using polarization gating²². It involves superposing left- and right-circularly polarized pulses separated by a small time-delay. In the region where the pulses overlap with equal amplitude, the superposition of the counter-rotating

fields results in a linear polarization. Since recollision is extremely sensitive to the ellipticity of the driving field²³, attosecond pulse emission is confined to this overlap region, resulting in the emission from a single half optical cycle (i.e. an isolated attosecond pulse) only.

Several variants of *in situ* measurement exist^{10,12}, each of which perturbs the recollision process and projects a signal containing information regarding recollision dynamics on either background-free spectral regions or spatial directions of the unperturbed experiment. For our experiment, we use a non-collinear method in which the perturbing field angularly deflects attosecond pulse emission²⁴. The deflected beam structure depends on the recollision dynamics and, thus, information is projected onto unused directions of the unperturbed attosecond pulse. It is ideally suited for characterizing isolated attosecond pulses²⁴. The experimental diagram is shown in Figure 1 (a). We focus a 12 fs, polarization gated driving pulse with central wavelength of 1.8 μm into an argon gas jet, as shown by the red pulse. The pulse reaches an estimated peak intensity of $1 \times 10^{14} \text{ W cm}^{-2}$ within the jet.

We perturb recollision with a second harmonic of the driving pulse that is polarized parallel to the linearly polarized component of the driving field. The perturbing pulse has an intensity of 10^{-4} of the driving field and is incident at an angle of 6.9 mrad with respect to the driving beam. It is delayed by a time τ , as depicted by the blue pulse in Fig. 1(a). In the gas jet, the perturbing field modifies the recollision trajectories, resulting in a frequency-dependent change of the near-field attosecond pulse wavefronts and propagation angle. As the delay between the perturbing and strong fields is varied, the angular deflection of each spectral component of the extreme ultra-violet (XUV) emission will modulate (by an angle θ in the figure in the far-field). The phase of this modulation is proportional to the XUV emission time¹². Figure 1 (b) shows the resultant spectrograms for XUV frequencies 60 (top) and 80 eV (bottom). The

difference in the modulation phase is proportional to the difference in XUV emission times for these energies. We have similar spectrograms for every frequency component.

The emission time analysis is performed for each spectral component of the measured attosecond pulse. The group delay of the recollision electron is obtained from the relative delay of each spectral component with respect to that of a fixed energy. Please see the methods section where this is discussed. The unperturbed attosecond pulse spectrum is shown in Figure 2 (a) in red, where the Cooper minimum is observed near 55 eV. The attosecond pulse spectrum from a TD-DFT simulation of the experimental conditions for the unperturbed attosecond pulse is shown by the dashed line (scaled $\times 10$ for clarity). The position of the Cooper minimum in the TD-DFT simulation, near 50 eV, is lower than the experimental result, but it is well-known that the position of the Cooper minimum in HHG is sensitive to phase-matching conditions²⁵. We use a thin gas jet to minimize contributions due to phase matching.

The measured group delay is shown in Figure 2 (b), where the experimental data is shown as a solid red line and the group delay of an attosecond pulse generated using our TD-DFT simulation of argon is shown by a dashed line. Since only relative group delays are determined, the absolute delay is unspecified. We chose that delay so that the experimental and theoretical curves are offset. Both the experimental and theoretical group delay curves are predominantly linear until the cut-off energy near 90 eV. Both, however, deviate from linearity near the Cooper minimum.

The difference between the experimentally measured group delay and the linear group delay expected from systems without a complex transition moment is the photorecombination time delay. Here, we use the group delay from a time-dependent Schrödinger equation simulation of a hydrogenic atom as our reference. For this simulation, we have modified the

ionization potential of hydrogen to 15.8 eV and all other parameters the same as those in the experiment. The difference between the measurement and simulated reference is shown in Figure 2 (c) in red and a smoothed version of the curve is shown in magenta. The maximum delay difference around the Cooper minimum near 54 eV is 160 as. The measured result agrees with other studies of photorecombination time delays in argon⁶.

We confirm this interpretation by simulating an *in situ* measurement using TD-DFT and a collinear second-harmonic perturbing field¹⁰ instead of the non-collinear geometry in the experiment. While the physics is the same, we note that, with collinear measurement, attosecond information is projected onto unused even-harmonic spectral components of the beam while information is projected onto unused directions of the beam for non-collinear methods. Thus, collinear fields require attosecond pulse trains. Here we use an attosecond pulse train to demonstrate the sensitivity of *in situ* measurement to the recombination phase while simultaneously taking advantage of the simpler collinear geometry for simulations.

With collinear fields, the perturbation breaks the half-cycle asymmetry of recollision, resulting in the emission of even harmonics¹⁰. The perturbation imparts a controlled phase difference between trajectories that are separated by half a laser period, thereby controlling the phase of photon emission at a given energy in adjacent half-cycles. This phase difference depends on the relative phase between the perturbing and driving fields. As the relative phase is scanned, the intensity of each even harmonic modulates periodically with a phase off-set proportional to its emission time and, therefore, the relative phase which maximizes (or minimizes) the even-harmonic signal is also proportional to the emission time¹⁰. This is discussed in the methods section. Both the non-collinear and collinear measurements rely on the

perturbation of recollision trajectories with a weak field and exhibit the same sensitivity to recollision dynamics^{12,24}.

We simulate high-harmonic generation in argon using an 800 nm driving pulse with a peak intensity of 2.75×10^{14} W cm⁻² and pulse duration of 20 fs, corresponding to a semi-classical cut-off near 70 eV. As in the experiment, we use a second harmonic intensity that is 10^{-4} of the fundamental and use an absorbing boundary to select short trajectories (see supplementary information). The Cooper minimum in high-harmonic generation is robust with respect to the driving field intensity and wavelength¹⁶ and we expect to see results similar to the measurement presented in Fig. 2.

The spectrogram from the simulated *in situ* measurement is plotted in Figure 3. The contour plot shows the normalized even harmonic spectrum plotted with respect to the relative phase between the driving and perturbing pulses on the left axis. The overlaid red line shows the maximizing relative phase for each even harmonic and the right axis shows the group delay calculated from the maximizing phase. The overlaid solid blue lines show the expected maximizing phase for recollision from an atom of ionization potential 15.8 eV with a constant transition moment phase (solid) and with a Lorentzian π -phase shift centred at 52 eV with a 10 eV bandwidth in its transition moment (dashed) calculated using the SFA²⁰ (both curves are shifted by $\pi/2$ for clarity).

The measured result deviates from the SFA result for the simple atom near the ionization threshold (i.e. below 25 eV) and around the Cooper minimum, where a prominent decrease in emission time is observed. The variation below 25 eV results from the variation of the Coulomb phase shift above the ionization threshold²⁶, which is not accounted for within the SFA. The linearity of the atomic result with a constant transition moment phase indicates that the variation

observed in the TD-DFT result around the Cooper minimum at 50 eV can be attributed to recombination effects. We verify this by comparing our measured result with the SFA result which includes a Lorentzian π -phase jump in its transition moment (see supplementary information). The maximizing phase calculated from the SFA when including this transition moment phase is shown by the dashed blue line and agrees with both the simulated and experimental *in situ* measurements.

The photorecombination delay is determined by finding the emission times for each even harmonic from the maximizing phase in Figure 3 and subtracting the expected semi-classical emission time. This is depicted in Figure 4 in red and compared with a reference calculated photorecombination delay in blue⁶. The photorecombination time delay from the simulated measurement exhibits a delay of nearly -175 as, in agreement with the experimental results in Figure 2. The differences between the simulated measurement and the reference photorecombination delay can be attributed to the energy resolution of the measurement technique and the interference of long and short trajectories near the high-harmonic cut-off of 70 eV²⁷. This validates our interpretation of the experimental measurement and demonstrates the feasibility of *in situ* techniques to measure photorecombination time delays.

The belief that *in situ* measurement cannot measure photorecombination time delay stems from studies¹¹ of photorecombination time delays due to molecular structure²⁸, where it was shown these time delays cannot be measured using attosecond *in situ* techniques. We demonstrate this apparent discrepancy encapsulates the critical difference between photoionization-based and *in situ* measurement. To understand why, it is useful to turn to the SFA. If we consider a simple atom, a recollision trajectory can be characterized by three parameters: the canonical momentum k , the time of ionization t_b , and the time of recombination

and photon emission t_r . If we perturbatively include a momentum-dependent transition moment phase, $\Phi_{tr}(k)$, the first-order correction to the emission time, $\Delta t_r^{(1)}$ is given as follows (atomic units are used):

$$\Delta t_r^{(1)} = \frac{1}{k + A(t_r)} \Phi'_{tr}(k + A(t_r)), \quad (1)$$

where $\Phi'(k) = \partial\Phi/\partial k$ and $A(t)$ is the vector potential of the driving field at time t .

When considering a molecular system, trajectories ionizing from and recombining to each atomic centre must be considered²⁹. When compared with a simple atom, the changes to individual trajectory emission times are the time required for an electron to travel the distance from the origin to the recombination atomic centre. For realistic internuclear separations, these changes are small. Only when all trajectories are superposed the emitted attosecond pulse exhibit a phase jump. Attosecond *in situ* methods characterize these trajectories individually instead of the emitted pulse. The effects of the internuclear separation cancel for *in situ* measurement (see supplementary information). This cancellation occurs for transition moment phases which vary linearly with the recollision electron momentum and for which the change in recombination is sufficiently small, as in phase shifts due to molecular structure. Thus, *in situ* methods are insensitive to molecular structure (see supplementary information).

The Cooper minimum is a result of the shape of the ground state wavefunction itself¹³ and is contained within a single path to recombination. Consequently, the correction to the recombination time reflects the shape of the phase jump and affects the trajectories which lead to attosecond pulse emission. This is shown in Figure 5 (a), which shows the electron trajectories calculated using the SFA leading to photon emission from 20 eV to 120 eV with a step size of 3.1 eV, for a system with a Lorentzian π -phase jump at 50 eV in its transition moment (please see supplementary information). The colour-scheme reflects the emitted photon energy for each

trajectory. The positions of ionization correspond to the position at which the electron exits the tunnelling barrier³⁰. The structure of the transition moment is reflected in the trajectories with emitted photon energies near 50 eV, where a variation in the position of recombination (solid dot marks) is observed.

Figure 5 (b) depicts the calculated recombination time delay (solid blue) and recombination position (dashed red) for each energy on the left and right axes, respectively. The shape of the recombination time delay is reflected in the variation of the recombination position. This variation in the recombination position can be understood by considering the nature of Cooper minima. Due to the radial nodal structure of the $3p$ orbital¹³, a spectral minimum occurs when the contributions to dipole emission from the inner (negative) and outer (positive) lobes of the radial orbital are equal. The inner lobe is tightly bound near the origin, while the outer lobe has an extent of ~ 10 a.u. For trajectories that ionize from the outer lobe but return with energies near 50 eV, dipole emission is dominated by the inner lobe, resulting in a change in recombination position of ~ 10 a.u.

Thus, the variation in the recombination delay can be directly mapped to the spatial structure of the ground-state wave function. In addition to the semi-classical action, the transition moment phase participates in establishing the phase matching conditions that determine which components of the recollision electron wave packet (i.e. trajectories) dominate dipole emission and, thus, are measured. This agrees with studies that show continuum and recombination dynamics are interrelated^{7,29,31} and calls into question the application of methods describing recollision which decouple propagation dynamics from recombination effects¹⁵.

In conclusion, both experimentally and theoretically, we have demonstrated an entirely optical measurement of photorecombination time delays by modulating recollision dynamics in

argon. Ours is a hybrid approach, in keeping with recollision, in which we exploit the optical coherence of high harmonic generation and the conceptual simplicity of a collision experiment. While photoionization and photorecombination are directly related in many ways, photoionization time delay measurements require a sophisticated photoelectron spectrometer in addition to the attosecond pulse generation apparatus¹⁴, hindering the widespread study of photoionization time delays. Furthermore, photoionization measurements are encumbered by the sensitivity to many possible sources of delay including electron dynamics^{3,6,7}, molecular structure^{5,11}, and dispersive effects during attosecond pulse propagation², leading to a lack of clarity of the meaning of the measurement.

In addition, our all-optical approach can be readily generalized to studying collision-induced plasmon excitation⁷, Fano resonances³² and other multielectron effects, extending to gas-phase molecules and possibly to solids. Since photoionization and photorecombination experiments measure different things, combining them will allow us to unambiguous isolation of time delays associated with molecular structure and electron dynamics effects. Any laboratory capable of generating high harmonics can perform these studies.

Finally, photorecombination time delay measurement open a new approach to attosecond pulse shaping in which the spectral phase structure of a passive external filter is replaced by the spectral phase structure of the transmission moment that can be controlled using external fields.

References

1. Goulielmakis, E. *et al.* Real-time observation of valence electron motion. *Nature* **466**, 739–743 (2010).
2. Cattaneo, L., *et al.*, U. Comparison of attosecond streaking and RABBITT. *Opt. Express* **24**, 29060–29076 (2016).
3. Du, T.-Y., Tang, D., Huang, X.-H. & Bian, X.-B. Multichannel high-order harmonic generation from solids. *Phys. Rev. A* **97**, 043413 (2018).
4. Varjú, K. *et al.* Frequency chirp of harmonic and attosecond pulses. *J. Mod. Opt.* **52**, 379–394 (2005).
5. Vozzi, C *et al.* Probing two-centre interference in molecular high harmonic generation. *J. Phys. B: At. Mol. Opt. Phys.* **39**, S457 (2006).
6. Schoun, S.B. *et al.* Attosecond pulse shaping around a cooper minimum. *Phys. Rev. Lett.* **112**, 153001 (2014).
7. Pabst, S. & Santra, R. Strong-field many-body physics and the giant enhancement in the high-harmonic spectrum of xenon. *Phys. Rev. Lett.* **111**, 233005 (2013).
8. Goldsmith, C., Jaroń-Becker, A. & Becker, A. Attosecond Streaking Time Delays: Finite-Range Interpretation and Applications. *Appl. Sci.* **2019**, 9, 492 (2019).
9. Nagele, S., Pazourek, R., Wais, M., Wachter, G. & Burgdörfer, J. Time-resolved photoemission using attosecond streaking. *J. Phys.: Conf. Ser.* **488** 012004 (2014).
10. Dudovich, N. *et al.* Measuring and controlling the birth of attosecond XUV pulses. *Nature Phys.* **2**, 781–786 (2006).
11. Spanner, M., Bertrand, J. B. & Villeneuve, D. M. *In situ* attosecond pulse characterization techniques to measure the electromagnetic phase. *Phys. Rev. A* **94**, 023825, (2016).
12. Kim, K.T., Villeneuve, D.M. & Corkum, P.B. Manipulating quantum paths for novel attosecond measurement methods. *Nature Photon* **8**, 187–194 (2014).
13. Cooper, J.W. Photoionization from outer atomic subshells. a model study. *Phys. Rev.* **128**, 681–693 (1962).
14. M. Sabbar, *et al.* Resonance Effects in Photoemission Time Delays. *Phys. Rev. Lett.* **115**, 133001 (2015)
15. Le , A.-T., Lucchese, R.R., Tonzani, S., Morishita, T. & Lin, C.D. Quantitative rescattering theory for high-order harmonic generation from molecules. *Phys. Rev. A* **80**, 013401 (2009).
16. Higuët, J. *et al.* High-order harmonic spectroscopy of the cooper minimum in argon: Experimental and theoretical study. *Phys. Rev. A* **83**, 053401 (2011).
17. Wong, M. C. H. *et al.* High harmonic spectroscopy of the cooper minimum in molecules. *Phys. Rev. Lett.* **110**, 033006 (2013).
18. Li, J., *et al.* 53-attosecond X-ray pulses reach the carbon K-edge. *Nat Commun* **8**, 186 (2017)
19. Maitra, N. Perspective: Fundamental aspects of time-dependent density functional theory. *J. Chem. Phys.* **144**, 220901 (2016).
20. Lewenstein, M., Balcou, Ph., Ivanov, M. Yu., L’Huillier, A. & Corkum, P.B. Theory of high-harmonic generation by low-frequency laser fields. *Phys. Rev. A* **49**, 2117–2132 (1994).
21. Corkum, P.B. Plasma perspective on strong field multiphoton ionization. *Phys. Rev. Lett.* **71**, 1994–1997 (1993).
22. Oron, D., Silberberg, Y., Dudovich, N. & Villeneuve, D.M. Efficient polarization gating of high-order harmonic generation by polarization-shaped ultrashort pulses. *Phys. Rev. A* **72**, 063816 (2005).
23. Flettner, A. *et al.* Ellipticity dependence of atomic and molecular high harmonic generation. *Eur. Phys. J. D* **21**, 115–119 (2002).
24. Kim, K.T. *et al.* Manipulation of quantum paths for space–time characterization of attosecond pulses. *Nature Phys* **9**, 159–163 (2013).

25. Farrell, J. P. *et al.* Influence of phase matching on the Cooper minimum in Ar high-order harmonic spectra. *Phys. Rev. A* **83**, 023420 (2011).
26. Pi, L.-W. & Landsman, A.S. Attosecond Time Delay in Photoionization of Noble-Gas and Halogen Atoms. *Appl. Sci.* **2018**, 8, 322 (2018)
27. Dahlström, J.M., L'Huillier, A. & Mauritsson, J. Quantum mechanical approach to probing the birth of attosecond pulses using a two-colour field. *J. Phys. B: At. Mol. Opt. Phys.* **44**, 095602 (2011)
28. Mauger, F. *et al.* High-harmonic spectroscopy of transient two-center interference calculated with time-dependent density-functional theory. *Structural Dynamics* **6**, 044101 (2019).
29. Labeye, M. *et al.* Dynamical distortions of structural signatures in molecular high-order harmonic spectroscopy. *Phys. Rev. A* **99**, 013412 (2019).
30. Daněk, J., Hatsagortsyan, K.Z. & Christoph H. Keitel. Analytical approach to Coulomb focusing in strong-field ionization. II. Multiple recollisions. *Phys. Rev. A* **97**, 063410 (2018)
31. Faccialà, D. *et al.* High-order harmonic generation spectroscopy by recolliding electron caustics. *J. Phys. B: At. Mol. Opt. Phys.* **51** 134002 (2018).
32. V. V. Strelkov, M. A. Khokhlova & N. Yu Shubin. High-order harmonic generation and Fano resonances. *Phys. Rev. A* **89**, 053833 (2014)

Figures

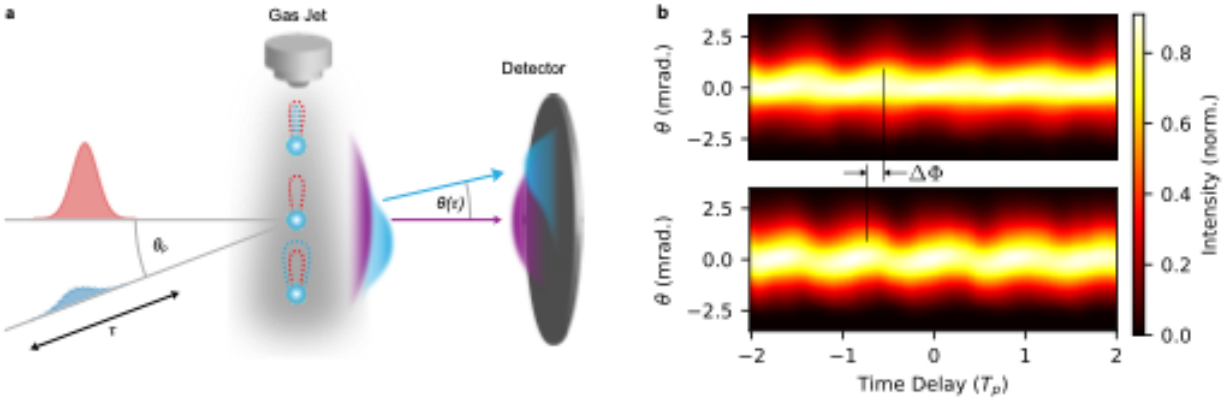


Figure 1 | Experimental diagram and analysis. (a) The polarization-gated driving pulse (red) and perturbing pulse delayed by time τ are focused into an argon gas jet. The perturbing pulse has a relative peak intensity of 10^{-4} and an incident angle of θ_p mrad with respect to the driving field. The perturbation induces a delay-dependent modulation of the electron trajectories across the beam front from red to blue dashed lines. The XUV wavefronts are modulated in the near field (from purple to blue), which results in a deflection of the XUV beam in the far-field by a delay-dependent angle $\theta(\tau)$. (b) The deflection of the XUV emission is recorded over a range of delays (in units of the perturbing field period T_p) and spectrally resolved. The resultant spectrograms for XUV energies of 60 eV (top) and 80 eV (bottom) are shown. The phase difference $\Delta\Phi$ of the deflection modulations is proportional to the difference in emission time, $\Delta\tau_\Omega$ between the two energies.

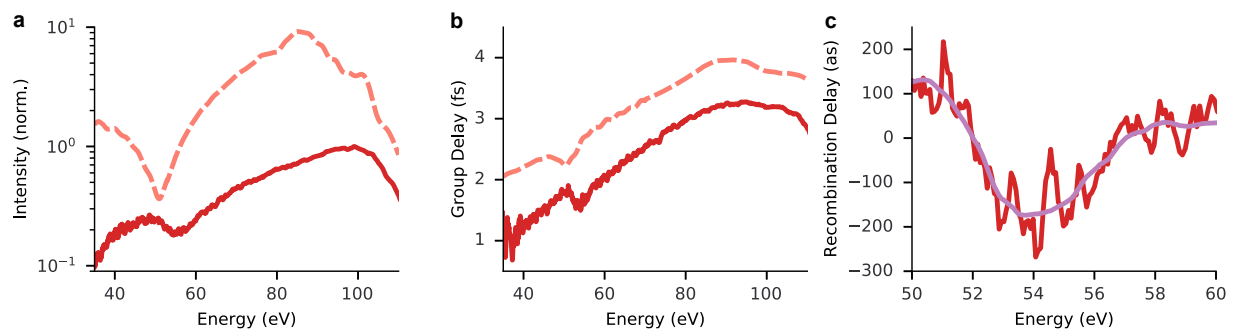


Figure 2 | Spectral intensity, group delay, and recombination delay. (a) Measured intensity spectrum and (b) group delay for the attosecond pulse generated in argon (solid line) by a 12 fs 1.8 μm driving field with a peak intensity of $1 \times 10^{14} \text{ W cm}^{-2}$. The dashed lines show the spectrum and group delay from a TD-DFT simulation of the experimental conditions. (c) Difference between the measured group delay and the expected semi-classical result in the spectral region of the Cooper minimum before (red) and after (magenta) smoothing the data.

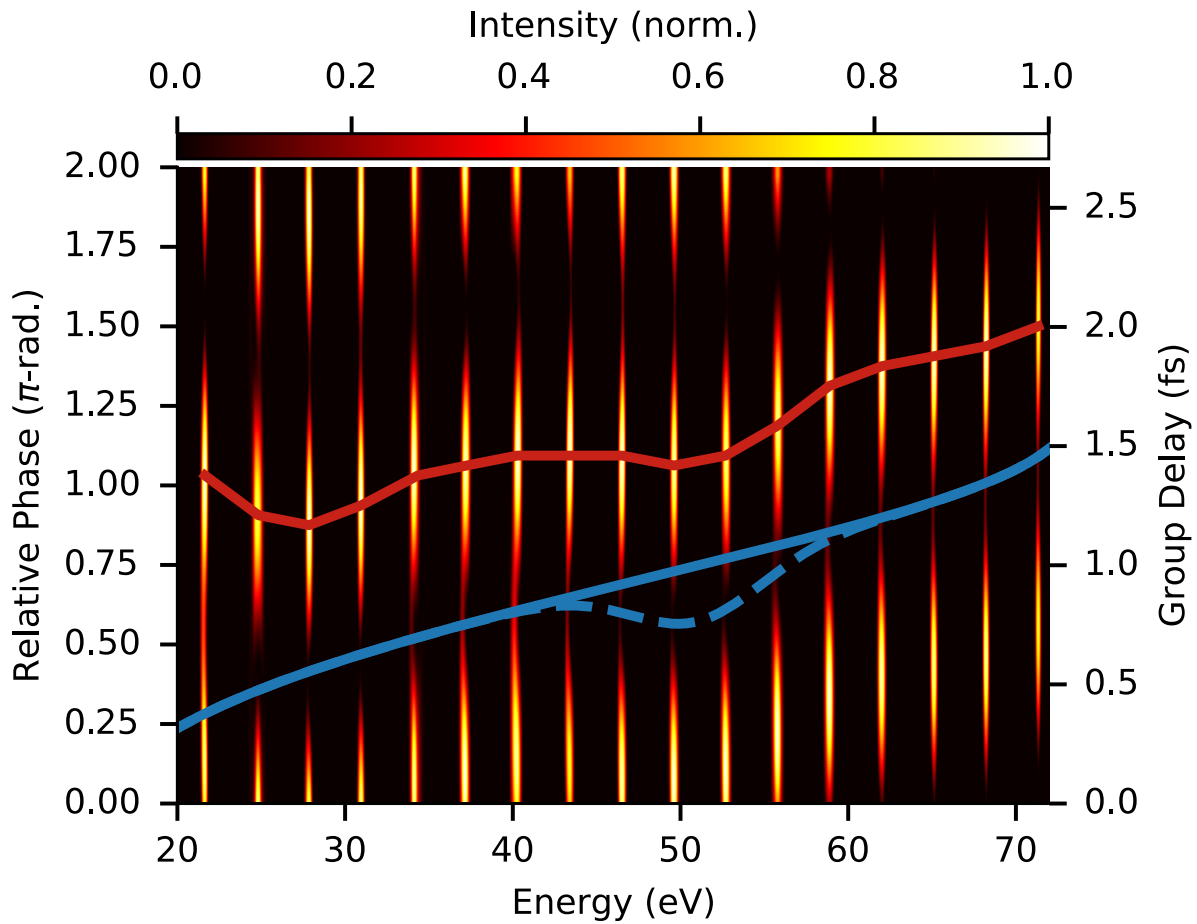


Figure 3 | Simulated collinear *in situ* spectrogram from argon. The normalized even-harmonic spectrogram from the TD-DFT simulation of an $\omega - 2\omega$ *in situ* measurement in argon. The overlaid red line shows the relative phase which maximizes each even harmonic signal from the simulation. The overlaid solid (dashed) shows the expected result for the maximizing relative phase from the semi-classical model without (with) the recombination phase around the Cooper minimum. The blue lines are shifted by $\pi/2$ for clarity. The driving field is an 800 nm pulse of duration 20 fs and peak intensity $2.75 \times 10^{14} \text{ W cm}^{-2}$ and the perturbing field is a second harmonic of the driving field with a relative intensity of 10^{-4} .

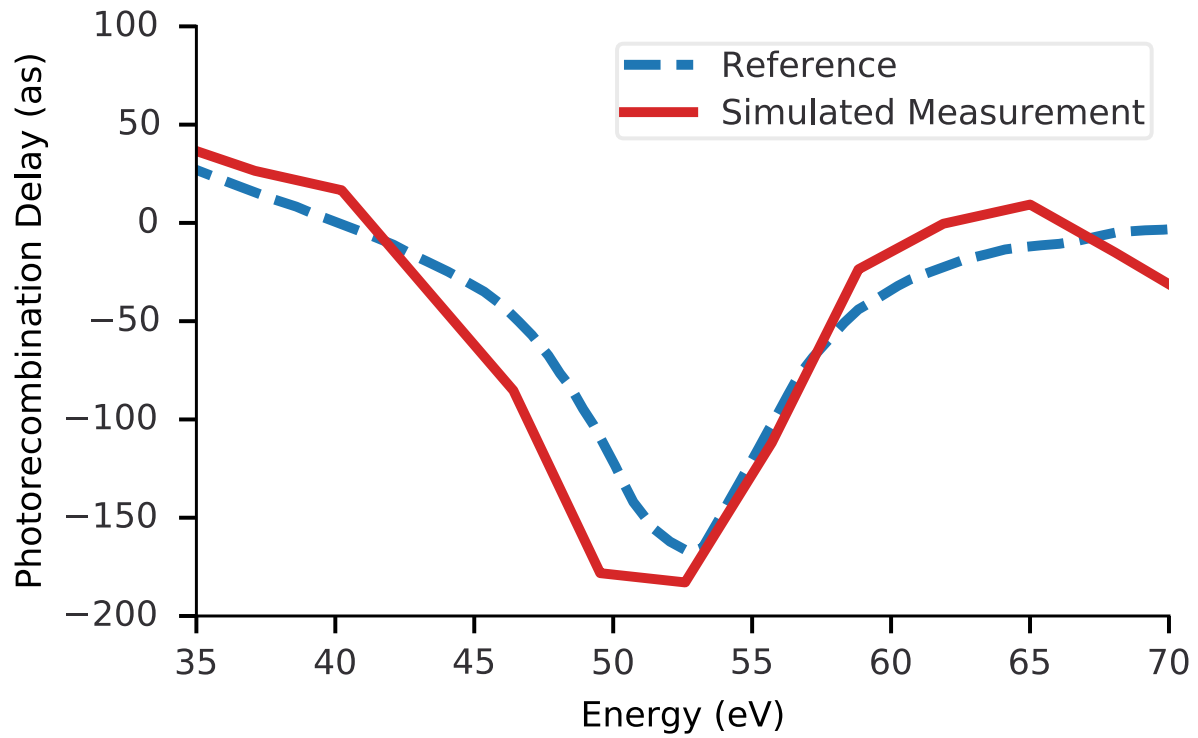


Figure 4 | Comparison of simulated *in situ* measurement photorecombination delay. A comparison of the photorecombination time delay reconstructed from the simulated spectrogram in Figure 3 (solid red) and calculated photorecombination time delay from argon around the Cooper minimum (dashed blue)⁶.

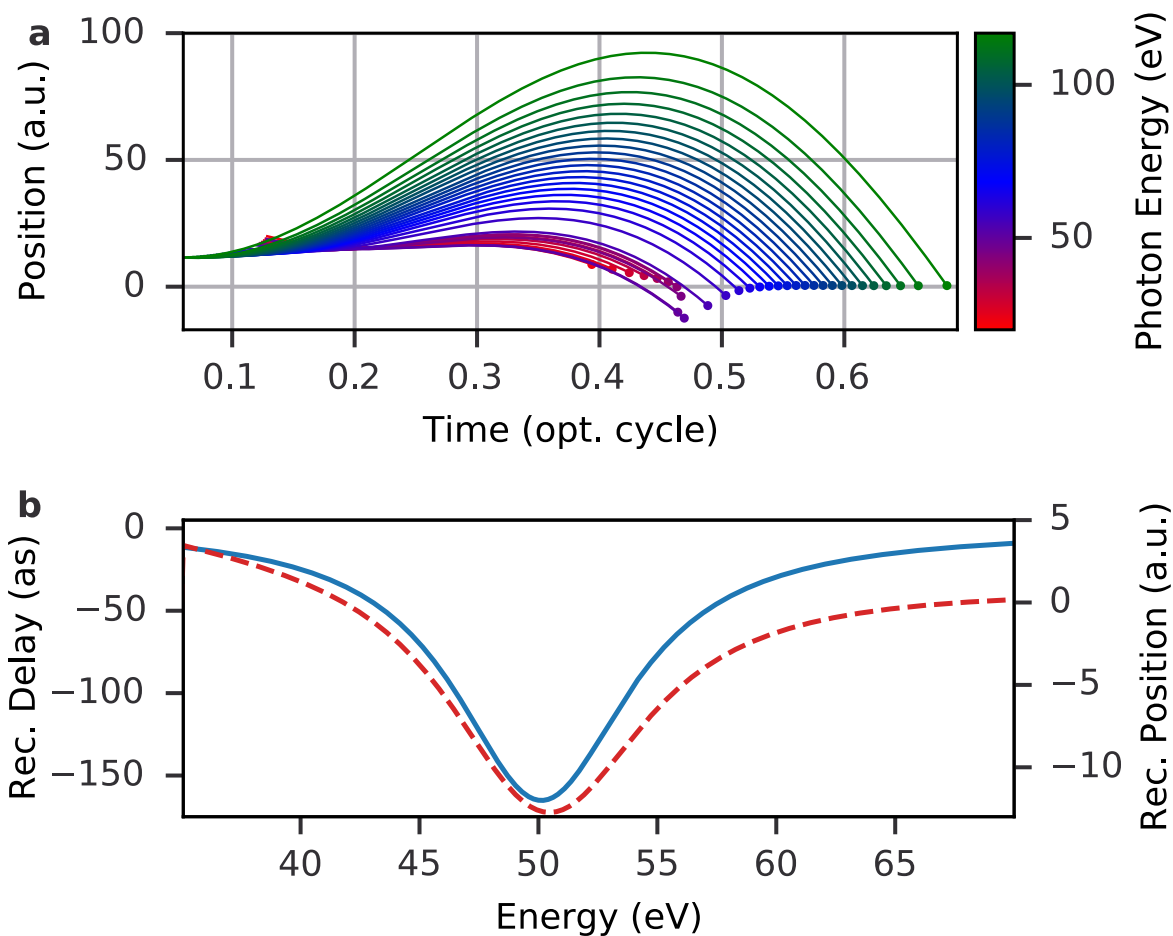


Figure 5 | The effect of the recombination phase on semi-classical trajectories. (a) Complex electron trajectories from an argon atom driven by a $1.8 \mu\text{m}$ field of intensity $1 \times 10^{14} \text{ W cm}^{-2}$ with a π -phase jump at 50 eV. (b) The recombination time delay (solid blue) and the variation in the position of recombination (dashed red) are shown on the left and right axes, respectively.

Methods

Experimental System

The 1.8 μm driving laser pulses in this experiment are delivered by a commercial optical parametric amplifier (HE-TOPAS, Light Conversion) which is pumped with a chirped-pulse-amplified Ti: Sapphire laser system (Thales, Alpha 100). The OPA system provides 50 fs laser pulses at 1.8 μm at a repetition rate of 100 Hz. The pulses are further amplified by a home-built OPA booster stage to get more than 1 mJ pulse energy and then focused into an argon-filled, differentially pumped hollow-core fibre (1 m long, 400 μm inside diameter) by a CaF_2 lens of focal length $f = 75$ cm. The spectrum is broadened with 0.8 bar argon gas in the hollow-core fibre and the residual chirp is compensated with an antireflection coated fused silica plate in the beam path. The spectrum after the propagation through the fibre is shown in Figure S1 (a). A pair of fused silica wedges is used for dispersion fine-tuning and controlling the carrier-envelope phase (CEP). We achieve 650 μJ sub-12 fs pulses from the fibre compressor, as shown in Figure S1 (b). The CEP of the 1.8 μm laser pulses was measured with a homebuilt f - $2f$ interferometer and locked by a servo system.

The laser beam after the fiber compressor is divided by a dichroic beam splitter after the second harmonic generation with a 200 μm -thick BBO crystal. The transmitted fundamental beam passed through a quartz plate with a thickness of 300 μm and a broadband quarter-wave plate to create a polarization gated beam for single attosecond pulse generation. The reflected second harmonic is of parallel polarization to the driving field and is used as a perturbing field in the XUV generation process. It is combined with the fundamental beam by a D shape mirror and the perturbation beam is positioned 2 mm below the fundamental.

Both beams are focused by a silver-coated concave mirror ($f = 30$ cm) into the gas jet. The angle between the two beams is ~ 6.7 mrad and their intensity ratio was $\sim 10^{-4}$. The time delay between two beams is controlled by a closed-loop piezo stage (Thorlabs) with a delay step of 66.4 as.

In the vacuum chamber, the gas source is from a pulsed argon gas jet with a backing pressure of 4.5 bars. The location of the gas jet is ~ 4 mm before the fundamental focus to enhance the short trajectory and a continuous spectrum extending from 30 eV to 110 eV is obtained.

The peak intensity at the focus is 5×10^{14} W cm^{-2} and the intensity at the jet position is estimated to be 1×10^{14} W cm^{-2} by the high harmonic cut-off. The high harmonics propagate through a slit, are frequency-resolved by a curved 1200 l/mm grating (Shimadzu, 30-002), and are recorded on a microchannel plate (Photonis, Chevron) with a charge-coupled device detector.

Experimental Temporal Characterization

The phase modulation induced by the perturbing field can be expressed as follows:

$$\sigma_{\Omega}(y, \tau) = A_{\Omega} \sin(k_p \theta_p (y - c\tau/\theta_p) + \Phi_{\Omega}),$$

where k_p is the perturbing pulse wavenumber of the perturbing field, θ_p is the relative angle between the perturbing and driving fields, y is the vertical position in the gas jet, c is the speed of light, τ is the delay between the perturbing and driving fields, and, for photon emission at frequency Ω , the terms A_Ω and Φ_Ω represent the frequency-dependent amplitude and phase of the modulation. The phase of the modulation depends linearly on the XUV emission time¹⁰. The difference in phase between two different frequencies can be directly observed from the XUV spectrum, as shown in Figure 1 (b), where this difference is mapped to a difference in emission, $\Delta\tau_\Omega$. The relative emission time of the entire spectrum is determined by determining the change in phase Φ_Ω from each spectral component's modulation relative to that of a fixed energy.

Simulated *In Situ* Measurement

For the simulated collinear *in situ* measurement, we consider HHG in Ar driven and perturbed by sinusoidal vector potential fields $A(t)$ and $A_p(t, \phi)$, respectively:

$$\begin{aligned} A(t) &= A_0 \sin(\omega_0 t), \\ A_p(t, \phi) &= \eta A_0 \sin(2\omega_0 t + \phi), \end{aligned}$$

where A_0 is the driving field amplitude, ω_0 is the fundamental field frequency, η is the relative amplitude of the perturbing and driving fields, and ϕ is the relative phase between the driving and perturbing fields. The phase modulation due to the perturbing field is given as follows¹⁰:

$$\sigma(t_r, \phi) = \Sigma(t_r) \cos(\phi - \theta(t_r)),$$

where t_r is the time of recombination, and $\Sigma(t_r)$ and $\theta(t_r)$ are found from the definition of the phase shift. For perfectly sinusoidal fields,

$$\theta(t_r) = \omega_0(t_r + t_b),$$

where t_b is the time of ionization. With this, the dipole moment leading to emission of harmonic $2N$ at time t_{2N} for integer N satisfies the following:

$$\tilde{D}(2N\omega_0) \propto \cos(\phi - \theta(t_{2N})).$$

The even-harmonic intensity modulates according to

$$|\tilde{D}(2N\omega_0)|^2 \propto \cos^2(\phi - \theta(t_{2N})),$$

which is maximized when

$$\phi = \theta(t_{2N}).$$

Thus, tracking the phases which maximize or minimize the even-harmonic signal provides a measurement of the harmonic emission time.

Further details of the experimental setup and theoretical simulations can be found in the supplementary information.

Data availability

The data that support the findings of this study are available from the corresponding author upon reasonable request.

Code availability

The codes used in this study are available from the corresponding author upon reasonable request. All requests should be made to G.G.B.

Acknowledgements

The authors would like to thank Drs. David Villeneuve and Michael Spanner for insightful discussions regarding attosecond *in situ* measurement and recombination dynamics. Their work and insights were invaluable in the development of our understanding of *in situ* measurement

This research was supported by the United States Air Force Office of Scientific Research (award #: FA9550-16-1-0109) with contributions from the Canada Foundation for Innovation, the Canada Research Chairs program, Canada's Natural Sciences and Engineering Research Council and the National Research Council of Canada.

Author contributions

C.Z. and D.H.K. designed the experiment. C.Z. performed the experiment. G.G.B. performed the numerical and semi-classical theoretical analysis. G.G.B. and C.Z. analysed the experimental data. G.G.B. and P.B.C. prepared the initial manuscript. All authors contributed in writing the manuscript. C.Z. and P.B.C. supervised the work.

Competing financial interests

The authors declare no competing financial interests.

Optical Measurement of Photorecombination Time Delays – Supplementary Information

Chunmei Zhang*, Graham G. Brown*, Dong Hyuk Ko, Paul B. Corkum

Joint Attosecond Science Laboratory, University of Ottawa and National Research Council of
Canada, 100 Sussex Dr, Ottawa, Canada, K1N 6N5

Corresponding Author Email: graham.brown@uottawa.ca

*These authors contributed equally to this work

April 26, 2021

Experimental Details

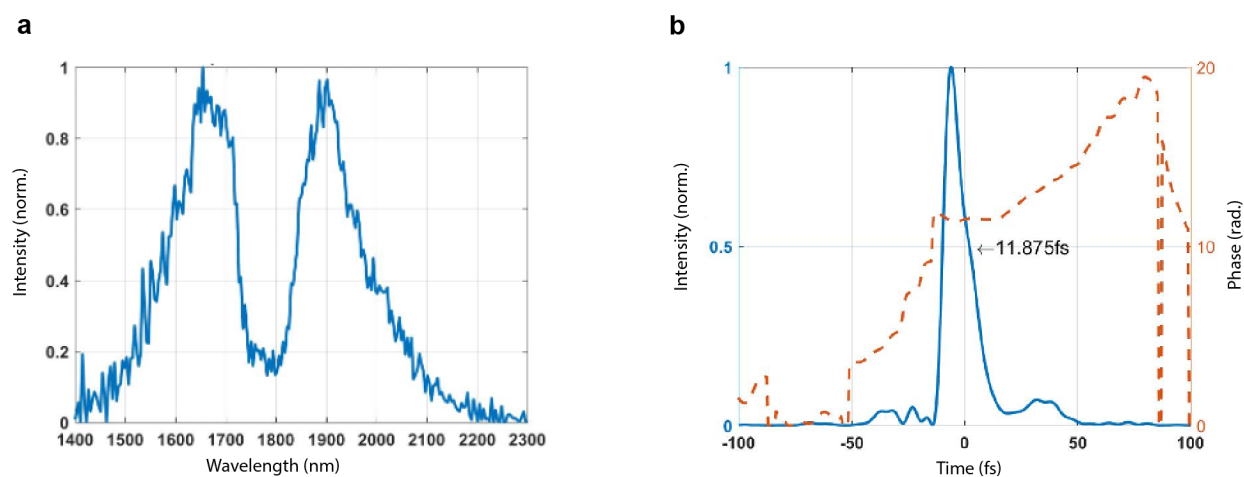


Figure S1 | Spectrum and temporal profile of driving field used in experiment. (a) The driving field spectrum at the exit point of the hollow-core fibre. (b) The temporal profile of the driving field pulse after compression of the pulse following propagation through the hollow core fibre.

The system used to generate an isolated attosecond pulse is described in detail in the Methods section of the main manuscript. Here, Figs. S1 (a) and (b) depict the spectral intensity and temporal profile of the driving laser, respectively, used in our experiment.

For the measurement of the attosecond pulse group delay, the non-collinear geometry results in a three-dimensional dataset including the attosecond pulse frequency, the time delay between the driving and perturbing fields, and the vertical position of the XUV beam. In the main text, we include two plots depicting the variation of the spatial properties along the vertical dimension of two frequency components of the attosecond pulse with the perturbing and driving field time delay.

Here, Fig. S2 depicts a spectrogram depicting the variation of the spectral intensity with the perturbing and driving pulse time delay at the central position of the unperturbed XUV beam.

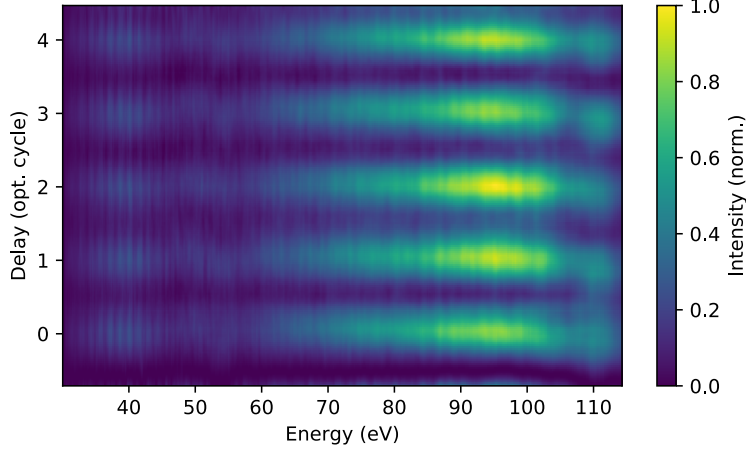


Figure S2 | On-axis *in situ* spectrogram of the spectral intensity. The variation of the spectral intensity with perturbing and driving field time delay measured at the central position of the unperturbed attosecond pulse.

The Strong-Field Approximation

The Effect of the Recombination Phase on Saddle-Point Solutions

We consider an atom with ground state $|\psi_0\rangle$, ionization potential I_p , and continuum states $|\mathbf{k}\rangle$ of momentum \mathbf{k} . Within the strong-field approximation, the dipole emission spectrum at frequency Ω , $\tilde{d}(\Omega)$, driven by a strong laser field of frequency ω_0 and polarized along the z-axis, $E_0(t) \hat{\mathbf{z}}$, is given as follows¹:

$$\begin{aligned} \tilde{d}(\Omega) = & -i \int d\mathbf{k} \int_{-\infty}^{\infty} dt_r \int_{-\infty}^{t_r} dt_b f^*(\mathbf{k} + \mathbf{A}_0(t_r)) e^{-i I_p(t_r - t_b) - iS(\mathbf{k}, t_b, t_r)} \\ & \times E_0(t_b) f(\mathbf{k} + \mathbf{A}_0(t_b)) e^{i\Omega t_r}, \end{aligned} \quad (S1)$$

where

$$f(\mathbf{k}) = \langle \mathbf{k} | \hat{z} | \psi_0 \rangle, \quad (S2)$$

$$S(k, t_b, t_r) = \frac{1}{2} \int_{t_b}^{t_r} [\mathbf{k} + \mathbf{A}(\tau)]^2 d\tau, \quad (S3)$$

where t_b is the time of birth and t_r is the time of recombination. We define the transition moment phase, $\Phi_{tr}(\mathbf{k})$, through the following:

$$\arg(\langle \mathbf{k} | \hat{z} | \psi_0 \rangle) = -\Phi_{tr}(\mathbf{k}). \quad (S4)$$

The total integrand phase, $\Phi_{tot}(\mathbf{k}, t_b, t_r, \Omega)$, is then the following:

$$\begin{aligned}\Phi_{tot}(k, t_b, t_r, \Omega) = & \Omega t_r - I_p(t_r - t_b) - \frac{1}{2} \int_{t_b}^{t_r} [\mathbf{k} + \mathbf{A}(\tau)]^2 d\tau \\ & - \Phi_{tr}(k + A(t_r)) + \Phi_{tr}(k + A(t_b)).\end{aligned}\quad (\text{S5})$$

The derivative of this phase with respect to the variables \mathbf{k} , t_b and t_r , respectively, yields a set of saddle-point equations:

$$0 = \int_{t_b}^{t_r} [\mathbf{k} + \mathbf{A}(\tau)] d\tau + \Phi'_{tr}(k + A(t_r)) - \Phi'_{tr}(k + A(t_b)), \quad (\text{S6})$$

$$0 = \Omega - I_p - \frac{[k + A(t_r)]^2}{2} + E(t_r)\Phi'_{tr}(k + A(t_r)), \quad (\text{S7})$$

$$0 = I_p + \frac{[k + A(t_b)]^2}{2} + E(t_b)\Phi'_{tr}(k + A(t_b)), \quad (\text{S8})$$

where $\Phi'(k) = \partial\Phi/\partial k$. The form of eqs. (S6-S8) suggest the transition moment phase acts equivalently to a spatial offset in the saddle-point equations.

The difference in the gradient of the transition moment phase in eq. (S6) acts as a displacement offset for the return condition, and as an energy shift in Eqs. (S7) and (S8) which describe energy conservation during ionization and recombination, respectively.

We consider recollision in an equivalent atom, but without a varying transition moment phase (i.e. $\Phi'(k) = 0$). We label the saddle-point solutions for the canonical momentum, time of birth, and time of recombination as \bar{k} , \bar{t}_b , and \bar{t}_r , respectively. We can then expand eqs. (S6 – S8) as a Taylor series with respect to $\partial\Phi_{tr}/\partial k$. To first-order, the corrections to the saddle-point solutions are as follows:

$$k^{(1)} = 0, \quad (\text{S9})$$

$$t_b^{(1)} = \frac{1}{\bar{k} + A(\bar{t}_b)} \Phi'_{tr}(\bar{k} + A(\bar{t}_b)), \quad (\text{S10})$$

$$t_r^{(1)} = \frac{1}{\bar{k} + A(\bar{t}_r)} \Phi'_{tr}(\bar{k} + A(\bar{t}_r)). \quad (\text{S11})$$

The presence of the transition moment in the saddle-point analysis will affect the prefactor within the SFA¹, although we omit this for brevity.

Recollision in Argon

We can approximate the phase variation across the Cooper minimum in argon as a Lorentzian π -phase jump centred at kinetic energy $K_0^2/2$:

$$\Phi_{tr}(k) = \arctan\left(\frac{k^2/2 - K_0^2/2}{\kappa^2/2}\right), \quad (\text{S12})$$

where $\kappa^2/2$ is the bandwidth of the phase jump. For the case of the Cooper minimum in argon, the variation of the transition moment phase varies sufficiently rapidly such that the first-order approximations used in Eqs. (S9-S11) are insufficient in describing the recollision dynamics. Consequently, we resort to numerical solutions of Eqs. (S6-S8) for the results presented in Figs. 3 and 5 of the main text.

Recollision in a Molecular System

We consider a molecule with two atomic centres separated by a distance R along the laser polarization axis². Setting the origin as the midpoint between the two atomic centres, the position of ionization and recombination can be described through the labels $\alpha = 1,2$ and $\beta = 1,2$, respectively. That is, ionization occurs at position $(-1)^\alpha R/2$ and recombination occurs at $(-1)^\beta R/2$. With this, the transition moment phase at the times of birth and recombination is given as follows:

$$\Phi_{tr}(k + A(t_b)) = [k + A(t_b)] \frac{(-1)^\alpha R}{2}, \quad (\text{S13})$$

$$\Phi_{tr}(k + A(t_r)) = [k + A(t_r)] \frac{(-1)^\beta R}{2}. \quad (\text{S14})$$

The corrections to the times of birth from atom α and recombination to atoms β for this system were derived elsewhere and we quote them here²:

$$t_{b,\alpha}^{(1)} = \frac{1}{k + A(\bar{t}_b)} \frac{(-1)^\alpha R}{2}, \quad (\text{S15})$$

$$t_{r,\beta}^{(1)} = \frac{1}{k + A(\bar{t}_r)} \frac{(-1)^\beta R}{2}. \quad (\text{S16})$$

Clearly, the spectral structure of the minimum in two-centre systems is not observed here. The magnitude of the corrections to the times of recombination decreases monotonically with electron kinetic energy and corresponds to the extra time required for an electron to travel a distance $(-1)^\beta R/2$. Most importantly, the abrupt phase jump observed in the emission spectrum is absent. Indeed, the spectral minimum results from the superposition of these four possible trajectories.

In the methods section of the main text, the procedure for a collinear *in situ* measurement is briefly described. The reader is encouraged to read ref. 10 for a more detailed description. When measuring recollision in a two-centre system using *in situ* techniques, the perturbation-induced phase shift for each trajectory closely resembles that from an equivalent atomic system. However, the transition moment phase for each trajectory varies linearly with the recollision electron momentum. Thus, the effect of the perturbing field on the transition moment will be of the same order as the effect on the semi-classical action and must be included when accounting for the perturbation-induced phase shift.

Since the changes to the saddle-point solutions are small, the change in the perturbation-induced phase due to the modified saddle-point solutions can be expanded to first-order in $\Delta t_{r,\beta}^{(1)}$. In doing so, the total perturbation-induced phase shift can be approximated as follows:

$$\sigma(k, t_b, t_r, \phi) \approx \sigma_0(\bar{k}, \bar{t}_b, \bar{t}_r, \phi) + \frac{E_p(\bar{t}_r, \phi) R^2}{\bar{k} + A(\bar{t}_r)} \frac{1}{4}, \quad (\text{S17})$$

where $\sigma_0(\bar{k}, \bar{t}_b, \bar{t}_r, \phi)$ is the perturbation-induced phase shift in an atomic system without a transition moment phase. The change to the perturbation-induced phase from the simple atomic case is proportional to the square of the recombination position and affects trajectories recombining to opposite atomic centres equally. Thus, the total *in situ* measurement will modulate according to eq. (S16), which does not reflect the structure of the spectral minimum due to two-centre interference.

This does not affect the measurement of the photorecombination time delay in argon, as the correction to the recombination time is significantly greater than in the case of two-centre interference. Consequently, the first-order approximations used here are insufficient in describing the measurement in argon and the influence of the perturbing field on the transition moment is negligible when compared with the change in the perturbation-induced phase shift due to the modified recombination times.

Description of Time-Dependent Density Functional Theory Simulations

The time-dependent Kohn-Sham equation in the absence of an external field is given as follows⁵:

$$i \frac{\partial \phi}{\partial t} = \left(-\frac{\Delta}{2} + v_0(\mathbf{r}) + v_h[n](\mathbf{r}, t) + v_{xc}[n](\mathbf{r}, t) \right) \phi(\mathbf{r}, t), \quad (\text{S18})$$

where Δ is the Laplacian operator, $v_0(\mathbf{r})$ is the external potential, $v_h[n](\mathbf{r}, t)$ is the Hartree potential (i.e. classical Coulomb repulsion between electrons), and $v_{xc}[n](\mathbf{r}, t)$ is the exchange-correlation potential. The radial grid is described using Gauss-Lobatto quadrature⁶. We work in spherical coordinates and the Kohn-Sham orbitals are expressed through a spherical harmonic expansion:

$$\phi_\alpha(r, t) = \sum_{l=m_\alpha}^{N_l} \phi_{\alpha,l}(r, t) Y_l^{m_\alpha}(\theta, \phi). \quad (\text{S19})$$

With this, the Hamiltonian for the time-dependent Kohn-Sham equation for each l -component of the α^{th} orbital is given as

$$\hat{H}_l(r, t) = -\frac{1}{2} \frac{\partial^2}{\partial r^2} + \frac{l(l+1)}{2r^2} + v_0^{(l)}(r) + v_h^{(l)}[n](r, t) + v_{xc}^{(l)}[n](r, t), \quad (\text{S20})$$

where the superscript (l) denotes the l^{th} multipole of each potential.

With g_α representing the occupation number of the orbital $\phi_\alpha(\mathbf{r}, t)$, the electron density is given as follows:

$$n(r, t) = \sum_{\alpha} g_{\alpha} |\phi_{\alpha}(\mathbf{r}, t)|^2. \quad (S21)$$

The expressions for the multipolar expansions of the Hartree potential are found through the multipolar expansion of the electron density⁷.

We use a generalized gradient approximation (GGA), LB94⁸. Exchange-correlation effects are only kept to the monopole order during time-propagation.

Transmission-free absorbing boundaries are used⁹. Time-propagation is implemented through the split-operator method¹⁰.

References

1. Lewenstein, M., Balcou, Ph., Ivanov, M. Yu., L'Huillier, A. & Corkum, P.B. Theory of high-harmonic generation by low-frequency laser fields. *Phys. Rev. A* **49**, 2117–2132 (1994).
2. Labeye, M. *et al.* Dynamical distortions of structural signatures in molecular high-order harmonic spectroscopy. *Phys. Rev. A* **99**, 013412 (2019).
3. Dudovich, N. *et al.* Measuring and controlling the birth of attosecond xuv pulses. *Nature Phys.* **2**, 781–786 (2006).
4. Spanner, M., Bertrand, J.B. & Villeneuve, D.M. In situ attosecond pulse characterization techniques to measure the electromagnetic phase. *Phys. Rev. A* **94**, 023825 (2016).
5. Maitra, N. Perspective: Fundamental aspects of time-dependent density functional theory. *J. Chem. Phys.* **144**, 220901 (2016).
6. Wang, J., Chu, S. & Laughlin, C. Multiphoton detachment of h^- . ii. intensity-dependent photodetachment rates and threshold behavior—complex-scaling generalized pseudospectral method. *Phys. Rev. A* **50**, 3208–3215 (1994).
7. J.D. Jackson. *Classical Electrodynamics*. 3rd Edition. Wiley, Hoboken (1999).
8. van Leeuwen, R. & Baerends, E. J. Exchange-correlation potential with correct asymptotic behavior. *Phys. Rev. A*, **49**, 2421–2431 (1994).
9. Manolopoulos, D. Derivation and reflection properties of a transmission-free absorbing potential. *J. Chem. Phys.* **117**, 9552 (2002).
10. Bauer, D. *Computational Strong-Field Quantum Dynamics*. De Gruyter GmbH, Berlin/Boston (2017).